Decoherence effects in the Stern-Gerlach experiment using matrix Wigner functions

P. Gomis* and A. Pérez†

Departamento de Física Teórica and IFIC, Universidad de Valencia-CSIC, Dr. Moliner 50, 46100-Burjassot, Spain

(Received 31 July 2015; revised manuscript received 28 April 2016; published 1 July 2016)

We analyze the Stern-Gerlach experiment in phase space with the help of the matrix Wigner function, which includes the spin degree of freedom. Such analysis allows for an intuitive visualization of the quantum dynamics of the device. We include the interaction with the environment, as described by the Caldeira-Leggett model. The diagonal terms of the matrix provide us with information about the two components of the state that arise from interaction with the magnetic field gradient. In particular, from the marginals of these components, we obtain an analytical formula for the position and momentum probability distributions in the presence of decoherence that shows a diffusive behavior for large values of the decoherence parameter. These features limit the dynamics of the present model. We also observe the decay of the nondiagonal terms with time and use this fact to quantify the amount of decoherence from the norm of those terms in phase space. From here, we can define a decoherence time scale, which differs from previous results that make use of the same model. We analyze a typical experiment and show that, for that setup, the decoherence time is much smaller than the characteristic time scale for the separation of the two beams, implying that they can be described as an incoherent mixture of atoms traveling in the up and down directions with opposite values of the spin projection. Therefore, entanglement is quickly destroyed in the setup we analyzed.

DOI: 10.1103/PhysRevA.94.012103

I. INTRODUCTION

The Stern-Gerlach (SG) experiment is a cornerstone in quantum mechanics. It showed, for the first time, direct evidence for the discretization of the spin states of the electron by analyzing the motion of silver atoms through a magnetic field gradient [1]. Most textbooks make continuous use of the SG as a simple way to illustrate the quantum measurement process, since the electron spin involves only a two-dimensional Hilbert space.

A consistent description of the SG experiment needs, obviously, to be quantum, even though one can make an introduction based on a semiclassical description using a spin-dependent force that gives rise to a "trajectory" which depends on the initial spin state. The full quantum treatment reveals a richer dynamics, as it leads to entanglement between the spin and spatial degrees of freedom [2–6].

In this paper, we perform a phase-space analysis of the SG device, including the interaction with the environment. This interaction will be described by the Caldeira-Leggett model [7]. In this respect, the starting point is similar to the analysis in [8]. However, our description is based on the use of the Wigner function (WF) [9]. Wigner functions have proven to be a powerful tool in physics and can be used as an alternative formulation of quantum phenomena, including their dynamics. The particular features of the phase-space description make it particularly advantageous in some situations, for instance, recognizing the quantum features of states, or dealing with decoherence scenarios. In the WF, interference effects manifest in a clear way [10–12].

In order to include the spin degree of freedom, one needs to extend the usual definition of the WF. A common prescription in the literature is the use of a matrix valued WF [13], where the spin indices give rise to the matrix elements. Such a description has some advantages when dealing with a particle subject to a spin-dependent force, since some effects like the spin precession, or motion that depends on the spin component, are better visualized with respect to a fixed spin basis. Examples of this description are a previous analysis of the SG experiment without including decoherence effects [14,15], the study of entangled vibronic quantum states of a trapped atom [13], or the reconstruction of the fully entangled quantum state for the cyclotron and spin degrees of freedom of an electron in a Penning trap [16].

As we will show, the phase-space description provides a clear visualization of the SG phenomenology. First, the diagonal terms show the motion of the two components of the quantum state (corresponding to spin up or down along the gradient direction). By considering an initial Gaussian state with arbitrary spin direction, we can obtain the marginals from the WF which describe the appropriate probability distribution function (PDF) of position or momentum [17]. Each of these PDFs have a Gaussian shape with a center and width which are modified by the interaction with the environment and give valuable information about the state evolution. On the other hand, the out-of-diagonal terms can be used to describe the effect of decoherence, which manifest into a damping of the norm associated to these terms. We use this norm as a figure of merit to quantify the amount of decoherence experienced by the system as a function of the parameter γ that quantifies the strength of the coupling with the environment. As a result, we obtain a decoherence time which scales as $\gamma^{-1/5}$, in contrast with previous results that claimed a $\gamma^{1/3}$ scaling [8]. We argue that our result is more realistic, as it implies that a larger decoherence parameter manifests into a shorter decoherence time scale. After considering a typical experiment, we show that, for such a setup, the decoherence time is much smaller than the characteristic time scale for the separation of the two beams, thus implying that these two beams can be described as an incoherent mixture of atoms traveling in the up and down direction with opposite values

*Pablo.Gomis@uv.es
†Armando.Perez@uv.es

of the spin projection. Therefore, entanglement is quickly destroyed in the experiment.

The rest of this paper is organized as follows. In Sec. II, we solve the equations that govern the evolution of the matrix WF for the SG device when the master equation based on the Caldeira-Leggett model is introduced to describe the environment. By evaluating the marginals of the diagonal elements, we obtain the position and momentum PDFs, and we analyze some limiting situations. Section III is devoted to the analysis of our results in a standard setup of the SG experiment. In particular, we study the damping of the off-diagonal terms and make use of this to define a decoherence time scale. Our conclusions are presented in Sec. IV, while some cumbersome expressions and extra calculations have been relegated to the Appendixes.

II. DYNAMICS OF MATRIX WIGNER FUNCTIONS INCLUDING INTERACTION WITH THE ENVIRONMENT

The behavior of a spin-1/2 neutral particle under the action of a magnetic field gradient, including the influence of decoherence effects, will be studied in this section. Particles entering the SG apparatus will move initially along the tube, defined as the x axis. The geometry of the magnetic field can be described by a dependence of the form

$$\vec{B}(x,y,z) = \eta y\vec{j} + (B_0 - \eta z)\vec{k}, \tag{1}$$

which contains a uniform part B_0 and a gradient of magnitude η on the plane orthogonal to the x axis. Notice that both position-dependent terms in the latter equation are necessary in order to satisfy $\vec{\nabla}\cdot\vec{B} = 0$ and $\vec{\nabla}\times\vec{B} = 0$. However, it can be shown that the effect of the magnetic field contribution along the y direction causes fast oscillations due to Larmor precession, which can be averaged out. Following [18], we neglect this contribution (see also [6]). In this way, in absence of decoherence effects, the problem can be effectively factorized as the free propagation along the x and y axis, and the nontrivial motion corresponding to the z coordinate, which can be described by the Hamiltonian

$$H = \frac{p^2}{2m} + \frac{2\lambda}{\hbar}(B_0 - \eta z)S_z, \tag{2}$$

where p is the canonical conjugate momentum for z, S_z is the third component of the spin operator, $\lambda = g_s\mu_B/2$, and m and g_s are the mass and gyromagnetic ratio of the particle, respectively. Finally, μ_B is the Bohr magneton.

In order to account for decoherence effects, we assume that they are described by the Caldeira-Leggett master equation [19], which accounts for those effects in the system via collisions with a thermal bath of particles. In the position and spin representation, with the Hamiltonian (2), the master equation can be written as [8]

$$\begin{aligned}\frac{\partial\rho_{\alpha\beta}(z,z',t)}{\partial t} = &\left[\frac{i\hbar}{2m}\left(\frac{\partial^2}{\partial z^2} - \frac{\partial^2}{\partial z'^2}\right) + \frac{i\lambda B_0}{\hbar}(\alpha-\beta)\right.\\ &- \frac{i\eta\lambda}{\hbar}(\alpha z - \beta z') - \gamma(z-z')\left(\frac{\partial}{\partial z} - \frac{\partial}{\partial z'}\right)\\ &\left.- \frac{D}{\hbar^2}(z-z')^2\right]\rho_{\alpha\beta}(z,z',t).\end{aligned} \tag{3}$$

In the latter equation, $\rho_{\alpha\beta}(z,z',t) \equiv \langle z,\alpha|\rho(t)|z',\beta\rangle$ are the matrix elements of the density operator $\rho(t)$ representing the particle state, at a given time t, on the basis $\{|z,\alpha\rangle \equiv |z\rangle\otimes|\alpha\rangle\}$, where $|z\rangle/z\in\mathbb{R}$ is the eigenbasis of the position operator and $\{|\alpha\rangle\}$ is a fixed basis in spin space. We find it convenient to choose the eigenstates of S_z ($|S_z = +\hbar/2\rangle = |+\rangle$, $|S_z = -\hbar/2\rangle = |-\rangle$) as the spin basis. Finally, γ is the damping rate of the system in the environment. The coefficient D is defined as $D = 2m\gamma k_B T$, with k_B the Boltzmann's constant and T the temperature of the environment.

As discussed in the Introduction, the analysis of the dynamics of this model will be presented on phase space, with the help of WF matrices

$$W_{\alpha\beta}(z,p,t) = \frac{1}{2\pi\hbar}\int_{-\infty}^{\infty} ds\, e^{-i\frac{ps}{\hbar}}\left\langle z+\frac{s}{2},\alpha|\rho(t)|z-\frac{s}{2},\beta\right\rangle, \tag{4}$$

where $W_{\alpha\beta}(z,p)$ are the spin matrix elements of the WF in the above-mentioned S_z base. The matrix WF has, among others, the following properties:

(1) One has

$$W_{\beta\alpha}(z,p,t) = W^*_{\alpha\beta}(z,p,t), \tag{5}$$

which implies that the matrix WF is Hermitian.

(2) The normalization condition becomes

$$\sum_\alpha\int_{-\infty}^{\infty}\int_{-\infty}^{\infty} W_{\alpha\alpha}(z,p,t)dzdp = 1. \tag{6}$$

(3) The marginal distributions of (4) are related to matrix elements of the density operator. In particular, for the diagonal components we have

$$\int_{-\infty}^{\infty} W_{\alpha\alpha}(z,p,t)dp = \langle z,\alpha|\rho(t)|z,\alpha\rangle \equiv f^{(\pm)}(z,t), \tag{7}$$

with $\alpha = \pm$, where $f^{(\pm)}(z,t)$ represents the position PDF for the particle. In a similar way, the marginal over the position variable

$$\int_{-\infty}^{\infty} W_{\alpha\alpha}(z,p,t)dz = \langle p,\alpha|\rho(t)|p,\alpha\rangle \equiv g^{(\pm)}(p,t) \tag{8}$$

represents the momentum PDF, with $|p,\alpha\rangle \equiv |p\rangle\otimes|\alpha\rangle$, $\{|p\rangle/p\in\mathbb{R}\}$ being the eigenstates of the momentum operator.

Using the definition Eq. (4) and the dynamics of the density matrix Eq. (3), one can obtain the corresponding differential equations for the WF matrix elements, given as follows:

$$\begin{aligned}\frac{\partial W_d^{(\pm)}(z,p,t)}{\partial t} = &-\frac{p}{m}\frac{\partial W_d^{(\pm)}(z,p,t)}{\partial z} + D\frac{\partial^2 W_d^{(\pm)}(z,p,t)}{\partial p^2}\\ &+\gamma\frac{\partial(pW_d^{(\pm)}(z,p,t))}{\partial p}\\ &\mp\eta\lambda\frac{\partial W_d^{(\pm)}(z,p,t)}{\partial p},\end{aligned} \tag{9}$$

$$\frac{\partial W_{od}(z,p,t)}{\partial t} = -\frac{p}{m}\frac{\partial W_{od}(z,p,t)}{\partial z} + D\frac{\partial^2 W_{od}(z,p,t)}{\partial p^2} + \gamma\frac{\partial(pW_{od}(z,p,t))}{\partial p} \pm \frac{2i\lambda(B_0+\eta z)W_{od}(z,p,t)}{\hbar}, \quad (10)$$

where $W_d^{(\pm)}(z,p,t)$ stands for the diagonal elements of the WF, with the upper sign corresponding to $W_{++}(z,p,t)$ and the lower sign to $W_{--}(z,p,t)$. We also defined $W_{od}(z,p,t) \equiv W_{+-}(z,p,t)$, which implies that $W_{-+}(z,p,t) = W_{od}^*(z,p,t)$, according to property 1 above.

A. General solution of the differential equations

To solve the system of equations (9) and (10), a Fourier transform is performed over both z and p [8]. The resulting equations can be solved with the help of the characteristics method [20]. Then, the WFs are retrieved by performing the inverse Fourier transform.

Assuming that the incident particles are described by a product state, consisting on a spatial Gaussian part, and a spin state $|n\rangle = a|+\rangle + b|-\rangle$ (with $|a|^2 + |b|^2 = 1$), the initial density operator $\rho(0)$ can be written as

$$\rho(0) = |\psi\rangle\langle\psi| \otimes |n\rangle\langle n|, \quad (11)$$

with the wave function that represents the initial state $|\psi\rangle$ in position space defined as

$$\psi(z) = \frac{1}{(\pi\sigma^2)^{1/4}} e^{-\frac{z^2}{2\sigma^2}}. \quad (12)$$

From the initial state Eq. (11) one obtains the matrix WF at $t = 0$, which can be written as

$$W(z,p,0) = \begin{pmatrix} |a|^2 & ab^* \\ a^*b & |b|^2 \end{pmatrix} W_i(z,p), \quad (13)$$

where

$$W_i(z,p) = \frac{e^{-\frac{\sigma^2 p^2}{\hbar^2} - \frac{z^2}{\sigma^2}}}{\pi\hbar} \quad (14)$$

represents the WF for a spinless Gaussian state, and σ is the Gaussian width of the particle's spatial PDF.

Solving the differential equation (9) by the method commented above, with the help of the initial condition (14), one finds the general solution for the diagonal elements. After some algebra, they can be written as follows:

$$W_d^{(\pm)}(z,p,t) = \frac{\gamma^2 m\sigma}{\pi\sqrt{G(\tau)}} e^{-\frac{F(z,p,\tau)}{G(\tau)}}, \quad (15)$$

and we have defined the new variable $\tau \equiv \gamma t$. The functions $F(z,p,\tau)$ and $G(\tau)$ are defined in Appendix A. In these functions we introduced the notations

$$z_c = \frac{\eta\lambda(\tau + e^{-\tau} - 1)}{\gamma^2 m}, \quad (16)$$

$$p_c = \frac{\eta\lambda(1 - e^{-\tau})}{\gamma}. \quad (17)$$

The role played by z_c and p_c will be discussed in the next section.

Using the same procedure for the differential equation (10), the solution for the off-diagonal elements is also found. The resulting expression is lengthy so that, in order to express it in a more compact way, we introduced the functions $C_i(\tau)$ ($i = 1,2,3,4,5,6$) that can be found in Appendix A. The off-diagonal elements can finally be written as

$$W_{od}(z,p,t) = \frac{e^{\left[\frac{2iB_0\lambda t}{\hbar} + C_1 - \frac{(-2C_2C_3\hbar + C_4C_5\hbar - iC_5z\hbar + 2iC_3p)^2}{4C_3\hbar^2(4C_6C_3 - C_5^2)} + \frac{(z+iC_4)^2}{4C_3}\right]}}{2\pi\hbar\sqrt{(4C_3C_6 - C_5^2)}}, \quad (18)$$

where we have omitted, for simplicity, the dependence of $C_i(\tau)$ on the variable τ. The matrix WF takes the following form:

$$W(z,p,t) = \begin{pmatrix} |a|^2\ W_d^{(+)}(z,p,t) & ab^*\ W_{od}(z,p,t) \\ a^*b\ W_{od}^*(z,p,t) & |b|^2\ W_d^{(-)}(z,p,t) \end{pmatrix}. \quad (19)$$

As we discuss below, the diagonal terms in $W(z,p,t)$ describe the behavior of the particles in phase space, and the off-diagonal terms represent the coherence of the state.

B. Marginals of the Wigner function: Position and momentum PDFs

The WF (for a spinless particle) cannot be associated with a probability distribution in phase space. In fact, it is referred to as a *quasiprobability distribution* and may even take negative values. This had to be expected from first principles, given the incompatibility of the position and momentum observables in quantum mechanics. One can, however, obtain the PDF corresponding to the particle position by integrating over the momentum variable, and vice versa, as described in the previous section. Equation (7) can be integrated, with the result

$$f^{(\pm)}(z,t) = \frac{e^{-\frac{(z\mp z_c)^2}{\sigma_z^2}}}{\sqrt{\pi}\sigma_z}, \quad (20)$$

where

$$\sigma_z^2 = \frac{2D(2\tau + 4e^{-\tau} - e^{-2\tau} - 3)}{\gamma^3 m^2} + \frac{\hbar^2(1 - e^{-\tau})^2}{\gamma^2 m^2\sigma^2} + \sigma^2 \quad (21)$$

is the squared width of the position distribution. Integration in Eq. (8) leads to the momentum PDF:

$$g^{(\pm)}(p,t) = \frac{e^{-\frac{(p\mp p_c)^2}{\sigma_p^2}}}{\sqrt{\pi}\sigma_p}, \quad (22)$$

with

$$\sigma_p^2 = \frac{2D(1 - e^{-2\tau})}{\gamma} + \frac{\hbar^2 e^{-2\tau}}{\sigma^2} \quad (23)$$

giving the squared width of the momentum distribution.

The above results for the marginals, Eqs. (20) and (22), clearly show that the diagonal components of the Wigner matrix correspond to Gaussian distributions in phase space (z,p) which center $(\pm z_c, \pm p_c)$ and width depend both on time,

and on the rest of the parameters of the problem, including the decoherence constants γ and D.

Let us notice the following properties of these quantities:

(1) By differentiating Eqs. (16) and (17) one readily obtains

$$\frac{dz_c}{dt} = \frac{p_c}{m}, \tag{24}$$

$$\frac{dp_c}{dt} = \eta\lambda - \gamma p_c, \tag{25}$$

which can be easily identified as the classical equations of motion for a particle subject to a constant force, plus a friction term. These equations allow us to describe the motion of the center of the two Gaussians using a semiclassical framework (especially if we neglect the interaction with the environment, as done in most textbooks).

(2) Let us consider the limit $\gamma t \ll 1$. Performing a Taylor expansion gives

$$z_c \simeq \frac{\eta\lambda t^2}{2m}, \quad \sigma_z \simeq \sigma + \frac{\hbar^2}{2m^2\sigma^3}t^2, \tag{26}$$

$$p_c \simeq \eta\lambda t, \quad \sigma_p \simeq \frac{\hbar}{\sigma} + \frac{\hbar}{\sigma}\left(\frac{2D\sigma^2}{\gamma\hbar^2} - 1\right)\gamma t. \tag{27}$$

If we further neglect the last term in Eq. (27), the above results can be easily interpreted as the action of a constant force on the particle and agree with the ones expected for the experiment in a decoherence-free environment [18].

(3) In the opposite limit (i.e., when $\gamma t \gg 1$) we can approximate

$$z_c \simeq \frac{\eta\lambda}{\gamma m}t, \quad \sigma_z \simeq \sqrt{\frac{8k_BTt}{\gamma m}}, \tag{28}$$

$$p_c \simeq \frac{\eta\lambda}{\gamma}, \quad \sigma_p \simeq \sigma_p^\infty \equiv \frac{2D}{\gamma} = \sqrt{4mk_BT}, \tag{29}$$

which leads to a limiting value of the momentum center (and width as well). This is a well-known effect in classical mechanics that appears under the action of a friction force and will play an important role in our analysis when large values of γ are assumed. We also obtain $\sigma_z \propto \sqrt{t}$, i.e., the characteristic behavior of a diffusive regime. Figure 1 features the evolution in time of the center of the PDF (both in position and momentum) using the values of the parameters as defined in the next section. For low values of γ, the center z_c of the position PDF first grows quadratically and then it grows linearly. The growth time scale is dictated by γ^{-1}, so that for very large values of this parameter z_c remains close to zero. On the other hand, the center p_c of the momentum PDF grows linearly for moderate values of γ but approaches a constant value as γ is increased, the asymptotic limit being inversely proportional to the decoherence parameter. In Fig. 2 we have plotted the width of the position and momentum distributions as a function of time. The position width σ_z grows quadratically for small values of t (as compared to γ^{-1}), whereas the regime $\sigma_z \propto \sqrt{t}$ corresponds to late times. The transition can only be seen for $\gamma = 1$ on this figure, given the γ^{-1} scaling. As for the plots representing σ_p, one can check that the ratio $\frac{2D\sigma^2}{\gamma\hbar^2}$ is of the order $\sim 10^{13}$. (Notice that this ratio is independent of γ.) Equation (27) then predicts a fast increase of σ_p even at early times, as it is clearly observed from these plots. This magnitude will then reach the asymptotic value σ_p^∞ also on the same γ^{-1} time scale, which can only be appreciated, in that figure, for the $\gamma = 10^{10}$ s^{-1} case.

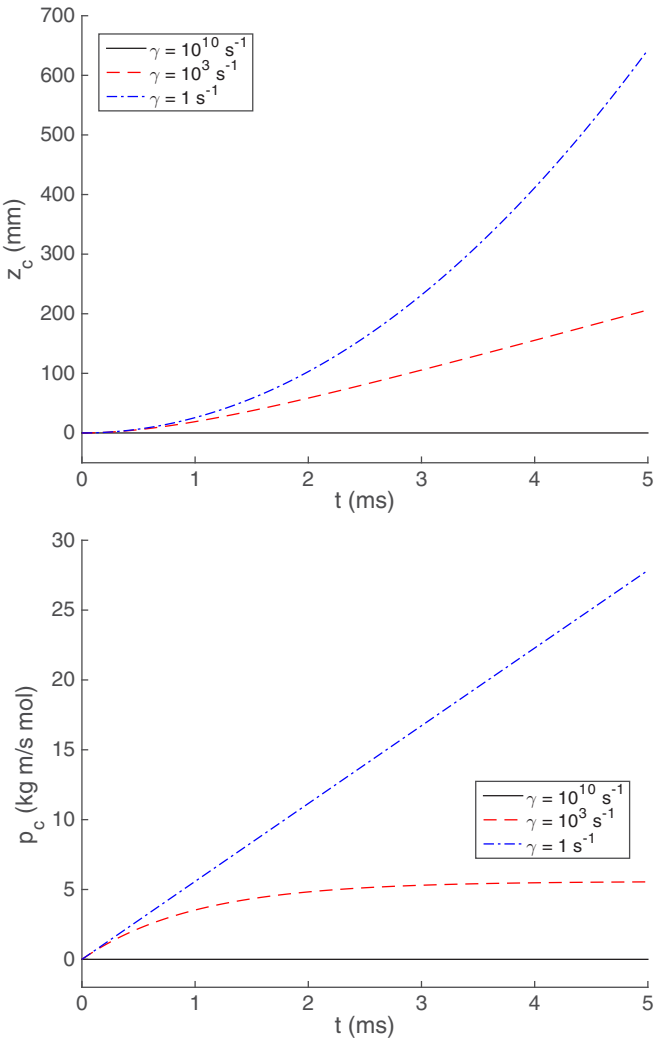

FIG. 1. Plots of the center of the position (up) and momentum (down) PDFs, as given by Eqs. (16) and (17), respectively, for three values of the parameter γ.

III. APPLICATION TO THE STERN-GERLACH EXPERIMENT

The study of a realistic SG experiment setup with decoherence effects will be the core of this section. First, parameters for the setup will be introduced. Then the evolution of the system will be pictured in phase space, using the results from the previous section. To conclude, the characteristic decoherence time of the system will be studied through the damping of the off-diagonal elements of the WF as the system evolves.

A. Experiment parameters

We assume an incident beam of silver atoms ($m = 1.8 \times 10^{-25}$ kg, $g_s \simeq 2$) starting in the $|S_x = \hbar/2\rangle = \frac{1}{\sqrt{2}}|+\rangle + \frac{1}{\sqrt{2}}|-\rangle$ spin state, with an average speed $v = 500$ m/s and a beam width $\sigma = 10^{-5}$ m. The SG apparatus parameters are

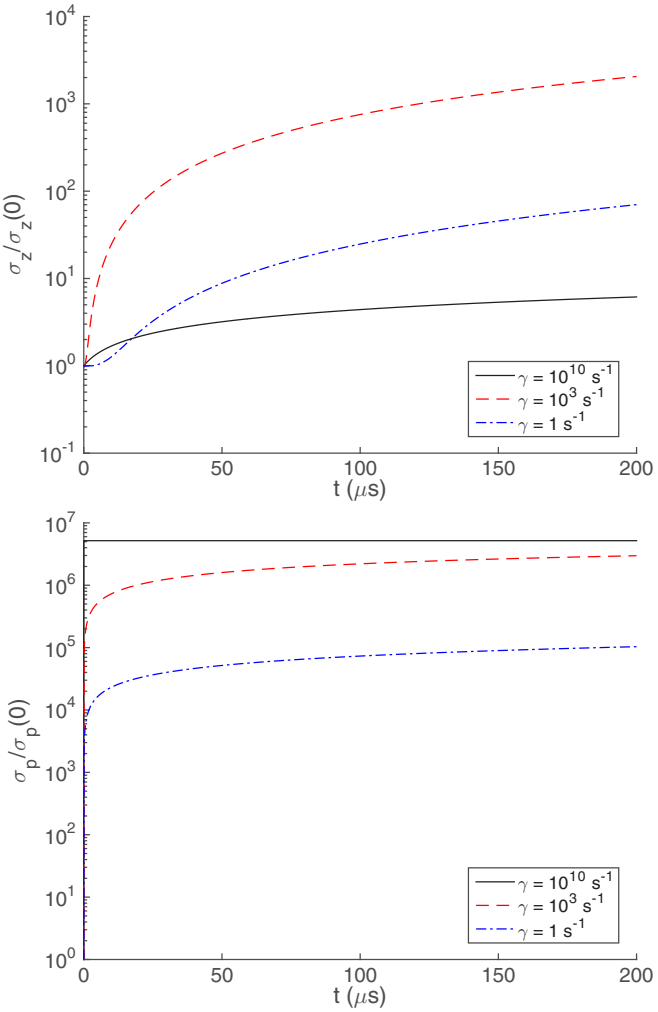

FIG. 2. Plots of the width of the position (up) and momentum (down) PDFs, for three values of the parameter γ.

based on the realistic ones used in a previous work [21]. In this setup, the applied magnetic field is $B_0 = 5$ T and the gradient $\eta = 1000$ T/m. The longitude of the tube is $l = 0.2$ m, which implies a flight time of around 0.4 ms for the above silver atom speed. This is, therefore, the characteristic time scale for the system dynamics. The operational temperature of the tube is around $T \simeq 300$ K, i.e., the laboratory temperature. The typical value for the pressure of the beam pipe is around $P \simeq 10^{-4}$ Pa [22].

The Langevin equation relates the damping rate γ of the Caldeira-Leggett master equation with the sum of viscous forces proportional to the silver's atom velocity v_z [23],

$$F_{\text{drag}} = -\zeta v_z, \tag{30}$$

where ζ is the so-called friction coefficient, from which γ can be obtained as

$$\gamma = \frac{\zeta}{2m}. \tag{31}$$

In order to calculate the drag force we need to calculate first the Knudsen number [24],

$$\text{Kn}(P,T) = \frac{2\lambda_a(P,T)}{D_s}, \tag{32}$$

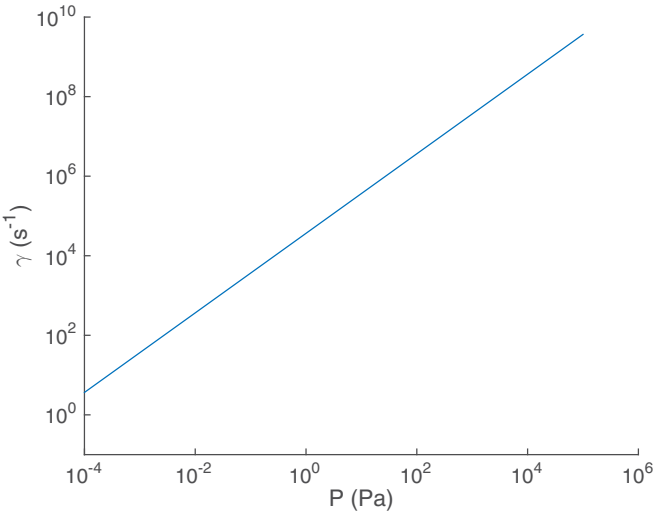

FIG. 3. Plot of the damping rate (γ), as defined by Eqs. (31) and (B1), as a function of the pressure, for a temperature $T = 300$ K.

where $\lambda_a(P,T) = \frac{k_B T}{\sqrt{2}\pi D_a^2 P}$ is the mean free path in the air, and $D_s = 288$ pm is the diameter of the silver atom. Assuming that the composition of the residual gas molecules in the beam pipe is similar to that of air at atmospheric pressure, we can estimate the diameter of the air molecule $D_a \simeq 0.4$ nm and its mass $m_a \simeq 5.610^{-26}$ kg.

We are interested in the pressure range from 10^{-4} to 10^5 Pa, for which we obtain that the Knudsen number ranges from 10^{11} to 10^3, respectively. For this high-Knudsen-number regime, we found that the best-suited framework to obtain the drag force on a silver atom is the one described in [25]. In their work, these authors develop a theory to calculate the motion of nonrigid spherical particles in low-density gases with Knudsen number $\text{Kn} \gg 1$.

The details of these calculations are discussed in Appendix B. From these results one can obtain, using Eq. (31), the damping rate as a function of the pressure in the beam pipe. The resulting γ values are plotted in Fig. 3. One observes that the damping rate can be well described as a linear function of the pressure for a fixed temperature (300 K), ranging from 3.7 s^{-1} at 10^{-4} Pa (the pressure at a typical SG experiment beam pipe) to 3.7×10^9 s^{-1} at 10^6 Pa (atmospheric pressure).

B. Phase-space representation

In this section we illustrate the behavior of the SG experiment in a decoherent environment by showing some plots of the WF using the parameters defined in Sec. III A for different values of the damping rate γ.

Three representative values, for three different regimes, will be considered: $\gamma = 1$ s^{-1} for the high-vacuum regime ($\sim 10^{-4}$ Pa), $\gamma = 10^3$ s^{-1} for the low-vacuum regime (~ 1 Pa), and $\gamma = 10^{10}$ s^{-1} for the atmospheric regime ($\sim 10^6$ Pa).

1. Diagonal elements

In order to represent the phase-space distribution of the particle, the trace of the matrix WF is plotted for $\gamma = 1$, 10^3, 10^{10} s^{-1} in Figs. 4, 5, and 6, respectively. The trace allows us to show the total quasiprobability distribution, thus putting on the same

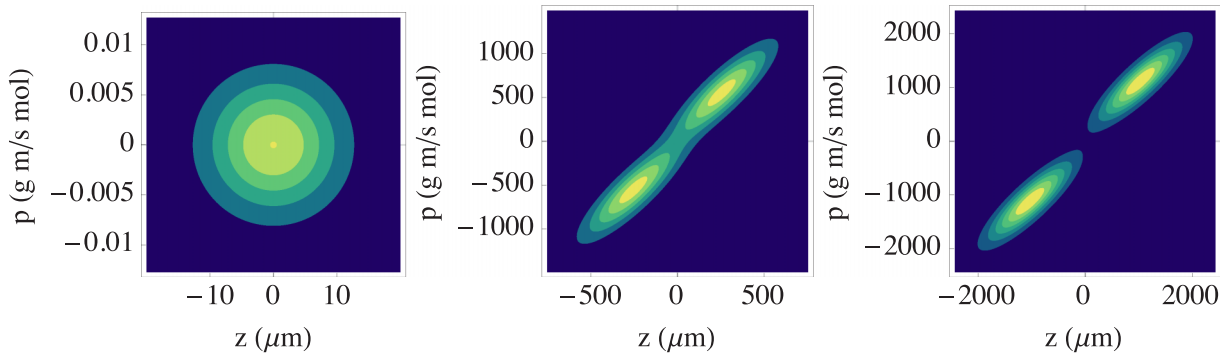

FIG. 4. Contour plots of the trace of the matrix WF with $\gamma = 1\ \mathrm{s}^{-1}$. The left panel corresponds to the initial ($t = 0$) state, while the middle panel shows the situation at $t = 100\ \mu$s, and the right panel is for $t = 200\ \mu$s.

plot both spin components. Figure 4 ($\gamma = 1\ \mathrm{s}^{-1}$) shows how the incoming state splits into two separating components within the experiment time scale (<1 ms). At $t = 100\ \mu$s both terms start to split, and at $t = 200\ \mu$s they are visibly separated. We observe the distortion of the original shape of the WF, caused by the different evolution in z and p, that appears even when the interaction with the environment is not included (see [14]). Note also that friction with the environment quickly broadens the spatial width, from the initial value $\sigma = 10^{-5}$ m to the millimeter scale in just $t = 200\ \mu$s. The same behavior can be observed for the momentum width.

As can be seen in Fig. 5 ($\gamma = 10^3\ \mathrm{s}^{-1}$), a higher value of the friction force quickly limits the momentum of the peak centers and causes the growth of the distribution widths. The influence of the SG apparatus is still visible in the shape of the beam, but due to the speed limit and the continuous growth of the width, the two components of the beam do not separate. An even larger value of the friction force (Fig. 6) causes the distribution peak centers to remain at the origin, and the width of the momentum distribution quickly grows, thus completely masking all the effects of the apparatus.

2. *Off-diagonal elements*

To study the off-diagonal WF, two three-dimensional (3D) plots of the real part of $W_{od}(z,p,t)$, corresponding to $\gamma = 1,\ 10^{10}\ \mathrm{s}^{-1}$, are drawn in order to see how the value of the damping constant affects the decoherence rate. At $t = 0$ (Fig. 7) this amounts to representing the initial Gaussian distribution Eq. (14).

As time goes on, Figs. 8 and 9 show how the real part of $W_{od}(z,p,t)$ evolves from a Gaussian distribution to an oscillatory pattern. We also observe that these oscillations are damped due to the interaction with the environment. By comparing both figures, we immediately see that a larger value of γ increases the oscillation frequency and reduces the amplitude of the oscillations, thus leading to a faster decoherence.

C. Decoherence time

In order to quantify the loss of coherence in the system we choose, as a figure of merit, the norm $\Delta(t)$ of $W_{od}(z,p,t)$ at a given t, defined as

$$\Delta(t) \equiv \int_{-\infty}^{\infty}\int_{-\infty}^{\infty} |W_{od}(z,p,t)|\ dz\ dp. \tag{33}$$

This quantity provides the total volume, in phase space, occupied by the coherent term of the WF. Taking the module, instead of the function itself, avoids cancellations due to the oscillatory nature of this term. In Fig. 10 we have plotted $\Delta(t)$ for different values of γ. As expected, decoherence effects manifest in a decrease of $\Delta(t)$ with time. In fact, the approach to zero appears at earlier times as one considers larger values of γ, clearly indicating a faster decoherence process.

In view of this result, we can introduce a decoherence time t_d as the time it takes for $\Delta(t)$ to reduce its initial value by a factor e. From the above data, we can obtain t_d for a given value of γ. These data are collected in Fig. 11.

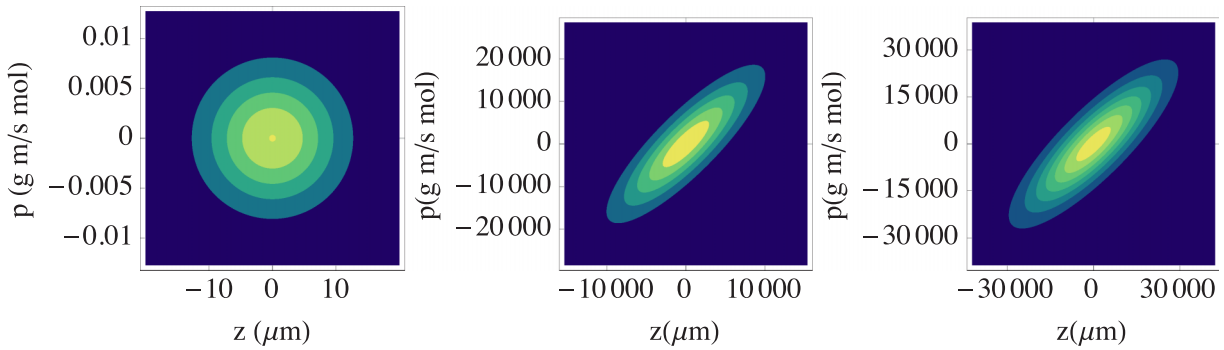

FIG. 5. Same as Fig. 4, for a value $\gamma = 10^3\ \mathrm{s}^{-1}$.

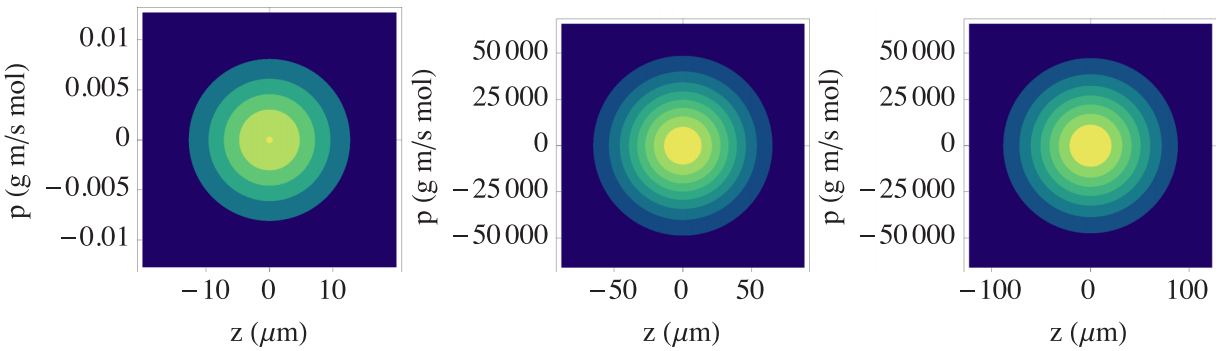

FIG. 6. Same as Fig. 4, using $\gamma = 10^{10}\ \mathrm{s}^{-1}$.

Performing a numerical fit to the curve $t_d(\gamma)$, we find that the decoherence time can be approximated by the formula $t_d = a\ \gamma^b$, with $a = (0.497 \pm 0.002)\ \mu\mathrm{s}$, and $b = -0.198 \pm 0.001$, pointing to a behavior as $t_d \propto \gamma^{-1/5}$. This result is at variance with the one discussed in [8], where a decoherence time given by $(\frac{3\hbar^2 m^2 \gamma^2}{4D\eta^2\lambda^2})^{1/3}$ was claimed, which translates into a dependence of the form $t_d \propto \gamma^{1/3}$, i.e., the larger the decoherence parameter γ, the later the system experiences decoherence. In our opinion, such a result is unrealistic, as one expects the opposite behavior: decoherence should take place faster as γ is increased, in accordance to our results.

This discrepancy arises from the criteria used to compute t_d. On the one hand, in [8] the solution found for the off-diagonal terms in the density matrix takes the form $\rho_{od} = e^{-(At+Bt^2+Ct^3)}$. It is then assumed that the term e^{-Ct^3} is the one that drives the coherence to zero. In this case, t_d is defined from the condition that the value of ρ_{od} is reduced by a factor e, which implies $t_d \sim C^{-1/3}$. On the other hand, in our calculations we computed the value of the norm's integral of $W_{od}(z,p,t)$ and we identified t_d as the time when the value of the integral decreases by an e factor, i.e., $\Delta(t_d) = e^{-1}\Delta(0)$.

In both cases t_d is defined as the time it takes the coherence to drop by a factor e. However, while it is true that the term e^{-Ct^3} will dominate in the limit $t \to \infty$, our results indicate that, in a realistic setup, other terms drive the coherence to zero before that term becomes relevant.

Returning to our results, as we obtain that the damping rate in our theoretical setup is around $3.7\ \mathrm{s}^{-1}$, the decoherence time according to our fit would be $t_d = 0.38\ \mu\mathrm{s}$. At that time, we expect the centers of the Gaussian packets to be separated by $z_c = 3.7$ nm, with a Gaussian width $\sigma_z = 10\ \mu$m, implying that in a typical Stern-Gerlach experiment, coherence is lost long before the separation of the Gaussian packages becomes measurable. This fact has important consequences concerning the interpretation of the experiment, at least for the setup adopted in our discussion. In fact, after a short time (given by the decoherence time), the WF will be approximated by

$$W(z,p,t) \simeq \begin{pmatrix} |a|^2\ W_d^{(+)}(z,p,t) & 0 \\ 0 & |b|^2\ W_d^{(-)}(z,p,t) \end{pmatrix}, \qquad (34)$$

which can be interpreted as describing an incoherent mixture of up-moving atoms with spin-up and down-moving atoms with spin down. This in turn implies that, although the spin-dependent interaction described by Eq. (2) tends to create an entangled state between spatial and spin degrees

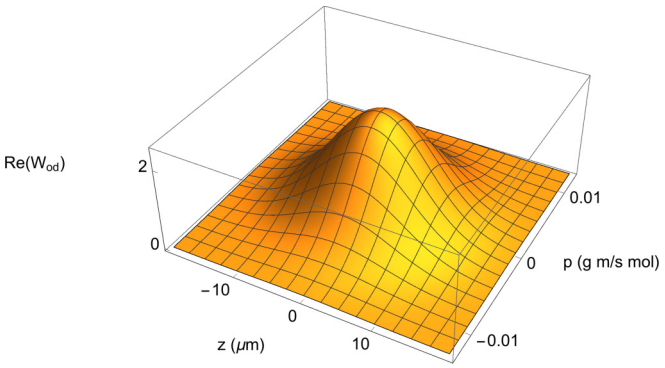

FIG. 7. 3D plot of the real part of $W_{od}(z,p,t)$ at $t = 0$.

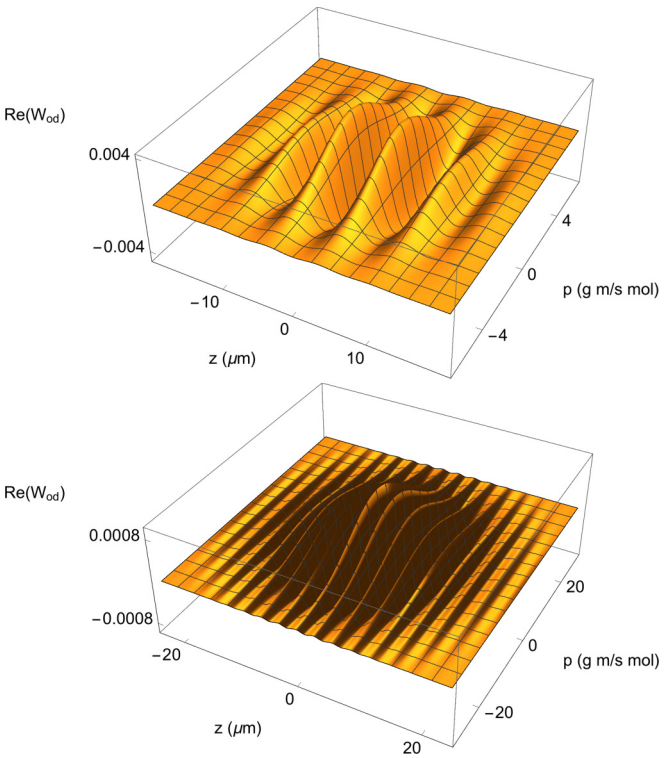

FIG. 8. 3D plot of the real part of $W_{od}(z,p,t)$ at $t = 0.005\ \mu$s (up) and $t = 0.1\ \mu$s (down), for $\gamma = 1\ \mathrm{s}^{-1}$.

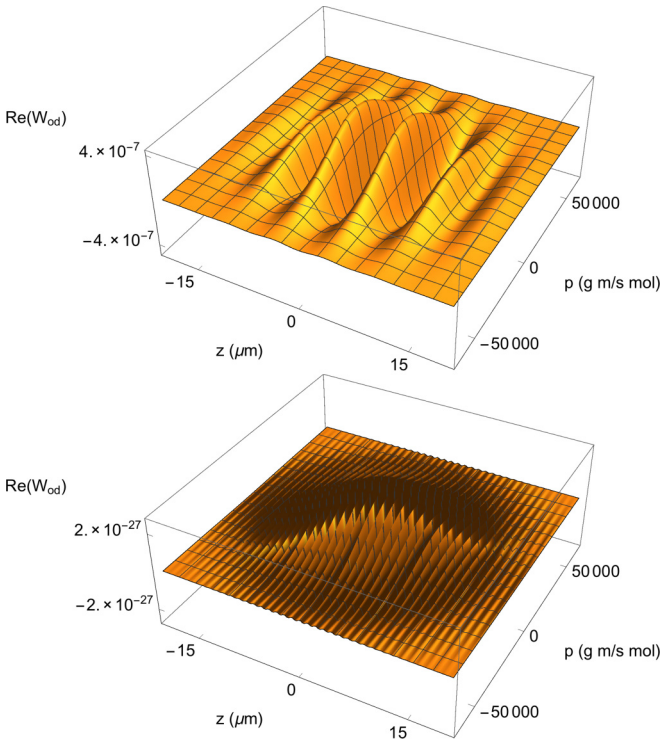

FIG. 9. Same as Fig. 8, for $\gamma = 10^{10}$ s^{-1}.

of freedom [2–6], decoherence will quickly degrade the built entanglement.

Our calculations are based on a model for which the system-environment interaction is spin independent. One might wonder if our conclusions can be substantially altered by the inclusion of a spin dependence on the damping rate γ and the diffusion rate D. While this would require to repeat all calculations starting from a different model, the following argument suggests that it may be very difficult to modify the

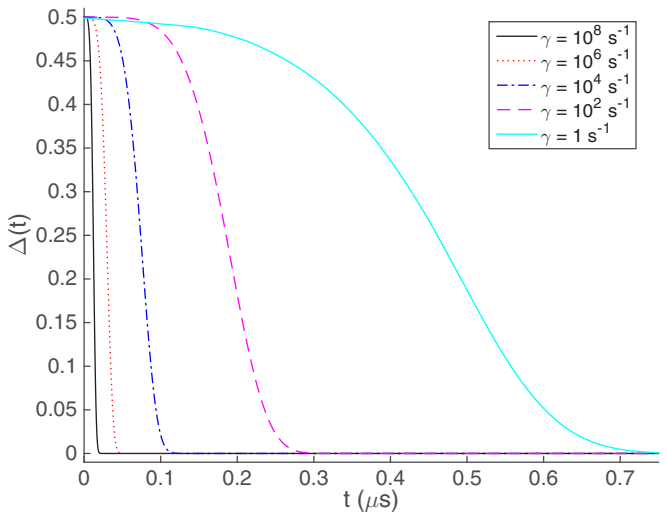

FIG. 10. Plot of $\Delta(t)$, as defined by Eq. (33), for different values $\gamma = 1, 10^2, 10^4, 10^6$, and 10^8 s^{-1} (curves from right to left) as a function of time.

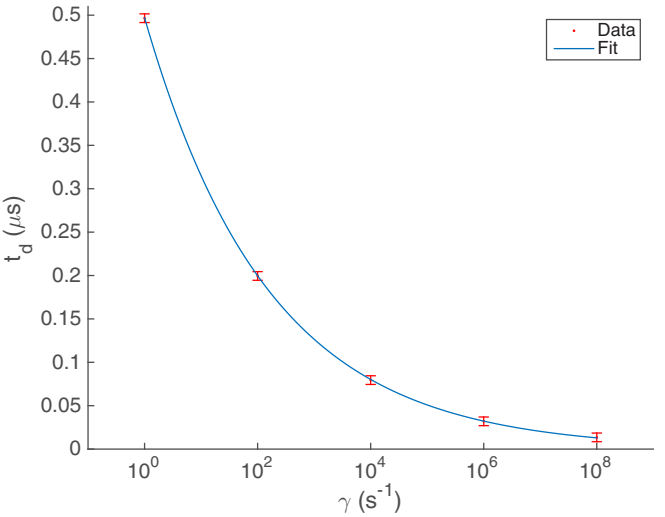

FIG. 11. Red points show the decoherence time t_d for the same values of γ used in Fig. 10. The bar indicates the imprecision that originates from the data. The solid curve is our fit $t_d = a\ \gamma^b$ (see the text for explanation).

present model such that the above results are dramatically changed.

Consider an alternative model where γ and D are still related by $D = 2m\gamma k_B T$, but γ shows an extra dependence on the spin direction. To simplify, we assume that this dependence takes the form of the spin operator S_x such that Eqs. (9) and (10) adopt the same form but with γ replaced by a different value γ' (and D by $D' = 2m\gamma' k_B T$) in (10). This implies that all equations concerning the dynamics of the position and momentum PDFs obtained in Sec. II B remain unchanged, while the discussion about decoherence effects developed in Sec. III C has to be recast in terms of γ' so that the decoherence time is parametrized as $t_d \simeq 0.5\ \gamma'^{-1/5} \mu$s. Since γ, which controls the dynamics of the diagonal components, is now independent of γ', we may wonder whether it is possible that the decoherence time becomes comparable to the time scale of the experiment, while keeping a similar value $\gamma \sim 1$ s^{-1}, so that the separation of both spin-up and spin-down components is visible. The characteristic flight time on the pipe is of the order $\sim$0.4 ms, from which one immediately obtains the condition $\gamma' \lesssim 10^{-15}$ s^{-1}. Such value is, therefore, many orders of magnitude lower than the ones found for γ in a typical experiment, which makes it very unlikely that a spin-dependent damping rate could substantially modify the above results. However, such spin-dependent effects might be relevant, within the model used along this work, for an improved setup in which γ is considerably lower, such that t_d becomes comparable to the flight time.

IV. CONCLUSIONS

In this paper, we have studied the SG experiment with environmental-induced decoherence described by the Caldeira-Leggett model. Our description is done on the phase space, making use of WFs, with the additional spin degrees of freedom. Our goal was to describe the kinematics of the atoms traversing the magnetic field gradient and interacting with a

thermal bath of particles, leading to Brownian motion and decoherence. We solved the differential equations for the WF corresponding to the model, starting from an *initial product state*, with a Gaussian shape in space, and an arbitrary spin direction. The diagonal terms on the S_z basis have a simple interpretation in terms of the two separating states of the apparatus. By calculating the marginals over momentum or position for each of the diagonal terms of the WF, we obtain the probability distribution for the conjugate variable. Each of the obtained diagonal distributions conserve the initial Gaussian shape, both in position and in space, in spite of the interaction with the environment, and allow for a clear description in terms of the center and width of the corresponding Gaussian, which bear a close analogy with the classical Brownian motion of a particle. In particular, at large times the particle reaches a limit velocity, a feature which is particularly important for the description of the SG experiment inside a gas tube. We also showed that our results agree with the nondecoherence expressions in the appropriate limit.

By adopting realistic parameters for the SG experiment, along with recent calculations for the interaction with atoms with a high-vacuum gas, we plotted the diagonal and off-diagonal elements of the WF. We observe that for low values of the decoherence parameter γ associated to high vacuum, the initial state separates into two components, corresponding to the up and down spin, as expected. The off-diagonal terms provide us information about decoherence, as a consequence of the interaction with the environment, that manifests in the damping of these terms as time evolves. In order to quantify the effect of decoherence, we evaluate the norm of the off-diagonal element over the whole phase space. The characteristic decoherence time scale t_d is defined as the instant when the initial norm is reduced by a factor e. By obtaining t_d for different values of γ, we find a relation that is well described by a power law $t_d \propto \gamma^{-1/5}$. Our finding differs from previous results, where a dependence $t_d \propto \gamma^{1/3}$ was claimed instead. We argue that such dependence is counterintuitive, as it would imply that a larger value of γ makes decoherence effects to appear later. In contrast, we obtain that a stronger value of γ implies a shorter decoherence time, which seems more reasonable.

The initial state for the silver atoms was assumed to be a product in spin and position. Under the effect of the Hamiltonian, one expects that entanglement between spatial and spin degrees of freedom will appear [2–6] at the beginning. However, given the values of parameters corresponding to the setup discussed in Sec. III A, we arrive at a characteristic decoherence time $t_d \sim 0.4\ \mu$s, which implies that, due to interaction with the environment, coherence is lost long before the separation of the Gaussian packets becomes measurable. As a consequence, the silver atom beam in the experiment is better described as an incoherent mixture of up-moving atoms with spin-up and down-moving atoms with spin down, so that entanglement, which is thought to be the fundamental resource in quantum information tasks, will inevitably be lost.

This conclusion, of course, does not prevent us from designing different setups where the decoherence time would be of the order (or perhaps larger) of the characteristic dynamical scale. Under such circumstances, one should observe the initial buildup of entanglement, followed by a transition towards an incoherent mixture. The observation of this kind of evolution is, thus, of potential interest for understanding the quantum-to-classical transition and will be the subject of a future study.

ACKNOWLEDGMENTS

This work has been supported by the Spanish Ministerio de Educación e Innovación, MICIN-FEDER Projects No. FPA2011-23897, No. FPA2014-54459-P, and No. SEV-2014-0398, and Generalitat Valenciana Grant No. GVPROMETEOII2014-087. We gratefully acknowledge useful conversations with J. A. Manzanares.

APPENDIX A: AUXILIARY FORMULAS FOR THE DIAGONAL AND OFF-DIAGONAL WIGNER FUNCTION

In this Appendix, we give explicit expressions for the auxiliary functions that define both the diagonal and off-diagonal terms of the matrix WF. The functions $F(z,p,\tau)$ and $G(\tau)$ that enter in the diagonal part, Eq. (15), are defined as

$$F(z,p,\tau) = 2\gamma D\sigma^2(\{\gamma^2 m^2(1-e^{-2\tau})z'^2 - 2\gamma m p'(1-e^{-\tau})^2 z' + p'^2[-(2-e^{-\tau})^2 + 2\tau + 1]\} + \gamma^4 m^2 p'^2\sigma^4 + \gamma^2\hbar^2[p'(1-e^{-\tau}) - \gamma m e^{-\tau} z']^2), \tag{A1}$$

$$G(\tau) = 8D^2\sigma^2(1-e^{-\tau})[(e^{-\tau}+1)\tau - 2(1-e^{-\tau})] + 2\gamma D\{\gamma^2 m^2\sigma^4(1-e^{-2\tau}) + [e^{-2\tau}(2\tau+3) - 4e^{-\tau} + 1]\hbar^2\} + \gamma^4 m^2\sigma^2 e^{-2\tau}\hbar^2, \tag{A2}$$

where $z' = z \mp z_c$, $p' = p \mp p_c$. The magnitudes z_c and p_c are given in Eqs. (16) and (17), respectively.

For the off-diagonal term defined in Eq. (18) we introduced the following definitions:

$$C_1(\tau) = \frac{\eta^2\lambda^2\{\sigma^2[-2D(2\tau^3 - 6\tau^2 + 6\tau + 3) + 6De^{-2\tau} + 24De^{-\tau}\tau - 3\gamma^3 m^2\sigma^2\tau^2] - 3\gamma(1-\tau-e^{-\tau})^2\hbar^2\}}{3\gamma^5 m^2\sigma^2\hbar^2}, \tag{A3}$$

$$C_2(\tau) = \frac{\eta\lambda[\gamma\hbar^2(e^{-\tau} - e^{-\tau}\tau - e^{-2\tau}) - 2D\sigma^2(1 - 2e^{-\tau}\tau - e^{-2\tau})]}{\gamma^3\hbar^2 m\sigma^2}, \tag{A4}$$

$$C_3(\tau) = \frac{\sigma^2[2De^{-2\tau} - 8De^{-\tau} - D(4\tau - 6) - \gamma^3 m^2\sigma^2] - \gamma\hbar^2(1-e^{-\tau})^2}{4\gamma^3 m^2\sigma^2}, \tag{A5}$$

$$C_4(\tau) = \frac{\eta\lambda[\gamma(1-e^{-\tau})(1-\tau-e^{-\tau})\hbar^2 - \sigma^2(2D(\tau+e^{-\tau}-1)^2+\gamma^3 m^2\sigma^2\tau)]}{\gamma^4 m^2\sigma^2\hbar}, \tag{A6}$$

$$C_5(\tau) = \frac{(e^{-\tau}-1)[\gamma e^{-\tau}\hbar^2 + 2D\sigma^2(1-e^{-\tau})]}{2\gamma^2 m\sigma^2\hbar}, \tag{A7}$$

$$C_6(\tau) = \frac{\gamma e^{-2\tau}\hbar^2 + 2D\sigma^2(1-e^{-2\tau})}{4\gamma\sigma^2\hbar^2}. \tag{A8}$$

APPENDIX B: CALCULATION OF THE DAMPING RATE IN ULTRALOW PRESSURE

In this Appendix, we describe a state-of-the-art calculation of γ for the conditions of our theoretical setup ($P \simeq 10^{-4} - 10^5$ Pa, $T = 300$ K), for pressures ranging from the beam pipe to atmospheric pressure. For this calculation, we start from the generalized formula of the drag force in the free-molecular regime discussed in [25] (see also [26]).

In their work, the authors find a generalization of the drag force for the free-molecular regime, using the kinetic theory, and obtain a formulation consistent with the Chapman-Enskog theory of molecular diffusion. Also, instead of assuming that the particles are rigid spheres moving through the gas, they assume a van der Waals interaction between the particles and the gas molecules. This van der Waals force includes forces among permanent dipoles, instantaneously induced dipoles, and permanent and induced dipoles. These forces are modeled through the Lennard-Jones potential.

These two features (agreement with the Chapman-Enskog theory, and use of the van der Waals interactions) make this theory best suited to calculate the drag force for a particle as small as an atom in low-density gases with Knudsen number $\mathrm{Kn} \gg 1$. The resulting formula found for ζ can be written as

$$\zeta = \frac{2}{3}\sqrt{2\pi m_r k_B T}\, N D_s^2 \Omega_{\mathrm{avg}}, \tag{B1}$$

where $m_r = \frac{m\, m_a}{m+m_a}$ is the reduced mass, $N = \frac{P}{k_B T}$ is the numerical density of residual air particles, and $\Omega_{\mathrm{avg}} = \varphi\Omega_d + (1-\varphi)\Omega_s$ is the effective reduced collision integral, which represents an average of the reduced collision integrals corresponding to diffusive and specular scattering, respectively, weighted by the momentum accommodation coefficient φ. These reduced collision integrals account for the influence of the interaction potential among the silver atoms and air molecules. They can be finally parametrized as [27]

$$\Omega_d = 1 + \frac{\pi}{8} + \left(1.072 + \frac{2.078}{T^{*1/4}} + \frac{1.261}{T^{*1/2}}\right)\sigma' + \left(3.285 - \frac{8.872}{T^{*1/4}} + \frac{5.225}{T^{*1/2}}\right)\sigma'^2, \tag{B2}$$

$$\Omega_s = 1 + \left(0.316 + \frac{1.47}{T^{*1/4}} + \frac{0.476}{T^{*1/2}}\right)\sigma' + \left(1.53 - \frac{5.013}{T^{*1/4}} + \frac{4.025}{T^{*1/2}}\right)\sigma'^2, \tag{B3}$$

$$\Omega_{\mathrm{avg}} = \frac{\Omega_d + \mathrm{Kn}(0.9\Omega_d + 0.1\Omega_s) - \frac{0.9\mathrm{Kn}(\Omega_d-\Omega_s)}{1+\left(\frac{D_s}{5}\right)^{15}}}{1+\mathrm{Kn}}, \tag{B4}$$

where $T^* = \frac{k_B T}{\varepsilon'}$ is the reduced temperature, and $\sigma' = \frac{2\sigma}{D_s}$ is the collision diameter. The effective well depth of the Lennard-Jones potential is defined as $\varepsilon' = \frac{2\pi\varepsilon\sigma^3}{3V}$, where $\varepsilon = \sqrt{\varepsilon_a\varepsilon_s}$, $\sigma = \frac{\sigma_a+\sigma_s}{2}$, and $V = \frac{m}{\rho_s}$ is the volume of a silver atom. The values of the Lennard-Jones potential parameters for air and silver are $\varepsilon_a/k_B = 98.4$ K, $\varepsilon_s/k_B = 3995.4$ K, $\sigma_a = 365.2$ pm, and $\sigma_s = 254$ pm. We use the value $\rho_s = 10\,500$ kg/m^3 for the density of the silver atom.

From the above data one can calculate the reduced collision integrals through Eqs. (B2) and (B3), obtaining $\Omega_d = 32.2$ and $\Omega_s = 29.6$ for a temperature of 300 K. The average of the collision integrals depends on the pressure through the Knudsen number. Using these results in Eq. (B1), we obtain the damping rate as a function of the pressure in the beam pipe. The results are plotted in Fig. 3.

[1] W. Gerlach and O. Stern, Eur. Phys. J. A **9**, 349 (1922).
[2] G. Reinisch, Phys. Lett. A **259**, 427 (1999).
[3] S. Cruz-Barrios, M. C. Nemes, and A. F. R. de Toledo Piza, Europhys. Lett. **61**, 148 (2003).
[4] M. Tumminello, A. Vaglica, and G. Vetri, Eur. Phys. J. D **36**, 235 (2005).
[5] J.-F. S. van Huele, B. C. Hsu, and J. R. Stenson, in *APS Meeting Abstracts* (2010), p. 42010.
[6] G. B. Roston, M. Casas, A. Plastino, and A. R. Plastino, Eur. J. Phys. **26**, 657 (2005).
[7] A. O. Caldeira and A. J. Leggett, Phys. Rev. Lett. **46**, 211 (1981).
[8] A. Venugopalan, D. Kumar, and R. Ghosh, Physica A (Amsterdam, Neth.) **220**, 563 (1995).
[9] E. Wigner, Phys. Rev. **40**, 749 (1932).
[10] N. Lee, H. Benichi, Y. Takeno, S. Takeda, J. Webb, E. Huntington, and A. Furusawa, Science **332**, 330 (2011).
[11] J. P. Dahl, H. Mack, A. Wolf, and W. P. Schleich, Phys. Rev. A **74**, 042323 (2006).
[12] M. Hillery, R. F. O'Connell, M. O. Scully, and E. P. Wigner, Phys. Rep. **106**, 121 (1984).
[13] S. Wallentowitz, R. L. de Matos Filho, and W. Vogel, Phys. Rev. A **56**, 1205 (1997).
[14] M. Utz, M. H. Levitt, N. Cooper, and H. Ulbricht, Phys. Chem. Chem. Phys. **17**, 3867 (2015).
[15] A. Reddy, J. Samuel, K. Shivam, and S. Sinha, Phys. Lett. A **380**, 1135 (2016).

[16] M. Massini, M. Fortunato, S. Mancini, P. Tombesi, and D. Vitali, New J. Phys. **2**, 20 (2000).
[17] W. P. Schleich, *Quantum Optics in Phase Space*, 1st ed. (Wiley-VCH, Weinheim, Germany, 2001).
[18] D. E. Platt, Am. J. Phys. **60**, 306 (1992).
[19] H.-P. Breuer and F. Petruccione, *The Theory of Open Quantum Systems* (Oxford University Press, Oxford, 2007).
[20] E. Zachmanoglou and D. Thoe, *Introduction to Partial Differential Equations with Applications*, Dover Books on Mathematics (Dover Publications, Dover, NY, 1986).
[21] M. Gondran and A. Gondran, Phys. Res. Int. **2014**, 605908 (2014).
[22] *Stern-Gerlach experiment*, Phywe Systeme GmbH & Co. KG, https://www.phywe.com/en/stern-gerlach-experiment.html.
[23] W. H. Zurek, Phys. Today **44**(10), 36 (1991).
[24] N. Marquardt, in *CERN Accelerator School: Vacuum Technology*, *Snekersten, Denmark, 1999: Proceedings*, edited by S. Turner (CERN, Geneva, Switzerland, 1999), pp. 1–24.
[25] Z. Li and H. Wang, Phys. Rev. E **68**, 061206 (2003).
[26] M. Li, G. W. Mulholland, and M. R. Zachariah, Phys. Rev. E **89**, 022112 (2014).
[27] Z. Li and H. Wang, Phys. Rev. E **68**, 061207 (2003).